Real-space collapse of a polariton condensate

L. Dominici,[1,2] M. Petrov,[3] M. Matuszewski,[4] D. Ballarini,[1] M. De Giorgi,[1] D. Colas,[5] E. Cancellieri,[6] B. Silva Fernández,[1,5] A. Bramati,[6] G. Gigli,[1,7] A. Kavokin,[8,9] F. Laussy,[5,9] and D. Sanvitto[1]

[1]*NANOTEC, Istituto di Nanotecnologia–CNR, Via Arnesano, 73100 Lecce, Italy*
[2]*Istituto Italiano di Tecnologia, IIT-Lecce, Via Barsanti, 73010 Lecce, Italy**
[3]*SOLAB, Spin Optics Lab, St. Petersburg State University, 198504 St. Petersburg, Russia*
[4]*Institute of Physics, Polish Academy of Sciences, Al. Lotnikow 32/46, 02-668 Warsaw, Poland*
[5]*IFIMAC, Física Teorica de la Materia Condensada, UAM, 28049 Madrid, Spain*
[6]*Laboratoire Kastler Brossel, UPMC-Paris 6, ÉNS et CNRS, 75005 Paris, France*
[7]*Universitá del Salento, Via Arnesano, 73100 Lecce, Italy*
[8]*CNR-SPIN, Tor Vergata, viale del Politechnico 1, I-00133 Rome, Italy*
[9]*Russian Quantum Center, 143025 Skolkovo, Moscow Region, Russia*

Polaritons in microcavities are versatile quasi-2D bosonic particles with a high degree of coherence and strong nonlinearities, thanks to their hybrid light-matter character[1]. In their condensed form[2], they display striking quantum hydrodynamic features analogous to atomic Bose-Einstein condensates, such as long-range order coherence, superfluidity[3] and quantized vorticity[4]. Their variegated dispersive and dissipative properties[5,6], however, set significant differences from their atomic counterpart[7]. In this work, we report the unique phenomenology that is observed when a pulse of light impacts the polariton vacuum: the condensate that is instantaneously formed does not splash in real space but instead coheres into an enigmatic structure, featuring concentric rings and, most notably, a sharp and bright peak at the center. Using a state-of-the-art ultrafast imaging with 50 fs time steps, we are able to track the dynamics of the polariton mean-field wavefunction in both real and reciprocal space. The observation of the real-space collapse of the condensate into an extremely localized—resolution limited—peak is at odd with the repulsive interactions of polaritons and their positive effective mass. An unconventional mechanism is therefore at play to account for our observations. Our modeling suggests that self-trapping due to a local heating of the crystal lattice—that can be described as a collective polaron formed by a polariton condensate—could be involved. These observations hint at the fascinating fluid dynamics of polaritons in conditions of extreme intensities and ultrafast times.

Microcavity polaritons have been praised for their fast response times[8,9] and ease of manipulation as well as detection, inherited by the photonic component, while keeping a strong nonlinear character[10], conferred by the excitons[6]. This makes them increasingly strong contenders in the field of interacting quantum fluids, where they have demonstrated the prevailing phases of strongly correlated systems[1], including Bose–Einstein condensation[2], superfluidity[3], e.g., scatterless flow, quantized vortices[4,11], together with rich spinorial patterns[12] and nonlinear interference effects. Polaritons have also demonstrated their suitability to investigate another mainstream concept fueled by dispersive and dissipative nonlinearities: shock waves and solitons, respectively characterized by step disturbances moving in the medium with sound velocity and by self-localization in space or shape preservation in time. Beyond polariton fluids[8,13–17], these have also drawn much attention in nonlinear media[18,19], atomic Bose-Einstein condensates (BECs)[20–27] or microcavities in general[28,29]. For instance, the response of a nonlinear medium or atomic BECs to an impinging blast resulting in the irradiation of shock waves[21,30], or the appearance of solitonic states[8] have been recently reported. Time-resolved exploration of such effects in strongly correlated gases remains largely unexplored and with the ultrafast imaging techniques now available, one is at the dawn of a new era for the investigation of quantum fluid dynamics.

While they have reproduced most of the known phenomenology of quantum gases, polaritons also come with peculiarities of their own, such as their dispersion relation or their short lifetime, making them intrinsically out-of-equilibrium. Here, we report what appears to be a unique phenomenology of these systems, observed after the sudden coherent generation of a polariton condensate. The fluid undergoes a space redistribution leading to a central localization of a great number of polaritons, despite their repulsive interactions. The peak that is formed reaches a localization ($\leq 2\mu$m, resolution limited) at least ten times sharper than the initial gaussian spot injected by the laser (18.5 μm). It also gathers a large number of particles, with a local enhancement up to 10 times the original density of polaritons. This striking dynamics takes place in a few ps. All these features can be tuned continuously with the excitation power. Another interesting feature of the dynamics is the generation of a shock wave at early times and concentric rings at later

*Electronic address: lorenzo.dominici@gmail.com

times. Similar rings and shock waves have been observed in nonlinear defocusing optical media or repulsive atomic BECs[19,25,30], but the presence of a central localised and enhanced peak has never been reported so far in any system, to the best of our knowledge.

The sample we used consists of a 2λ microcavity (MC) containing a triple quantum well (QW) positioned in the maxima of the electromagnetic field[3,10]. An excellent quality factor (photonic $Q = 14000$) is given by two high reflectance multilayers mirrors (DBR, distributed Bragg reflectors) embedding the MC. The strong coupling between the QW excitons and MC photons manifests itself as an anticrossing of their original modes splitting into two new normal modes, known as polaritonic upper (UPB) and lower (LPB) branches (see supplementary figure S5). All the experiments shown here are performed at zero detuning between the MC and the QW exciton, both resonant at ~ 836 nm, and in a region of the sample clean from defects in order to avoid any effect due to spatial inhomogeneities. The device is kept at a temperature of 10 K. We implemented an unltrafast imaging technique based on the off-axis digital holography[4,9,31,32] to study the dynamics of the polariton flow with spatial and temporal steps of 0.16 μm and 50 fs respectively. A 130 fs or 3.5 ps laser pulse, on resonance with the bottom of the LPB and circularly or linearly polarized, is directed onto the sample at normal incidence and the evolution of the polariton state in time is recorded by making interfere the sample emission with a delayed reference beam into a CCD camera. Digital elaboration in the reciprocal space of the interferograms allows to retrieve the complex wavefunction of the photonic emission, which is coherent with the polaritonic wavefunction, and thus allows us to image both the amplitude and phase of the light-matter fluid. For energy resolved images a standard 550 cm long spectrometer is used before the CCD and the spectra are time integrated. Additional details on the sample and the technique can be found in Ref.[9] and the supplementary material therein.

The dynamics of the polariton fluid, generated instantaneously by a resonant laser pulse hitting the sample, is shown in Fig. 1. Initially, the polariton distribution is simply a footprint of the incoming laser spot, i.e., a gaussian of 18.5 μm (FWHM). Panels (a-c) shown the sample emission at the pulse arrival, in density (a), amplitude (b) and phase (c). The unwrapped phase along a central diameter is shown in panel (d), with the shallow positive curvature associated to a weak outward gradient. The central density of polaritons is initially 550 μm^{-2}. For the first few ps, the fluid only slightly decreases its total number of particles—due to radiative losses—however, at ~ 2 ps, the maximum density suffers a sudden depletion, down to only a quarter of the initial density. This is shown in panels (e,f) for the intensity and (g,h) for the phase. This unanticipated jolt marks the beginning of the redistribution of the fluid. Note that the phase space profile starts to manifest a negative curvature with a reversal point of the phase gradient ($\nabla\phi$) at $r = 20\mu$m.

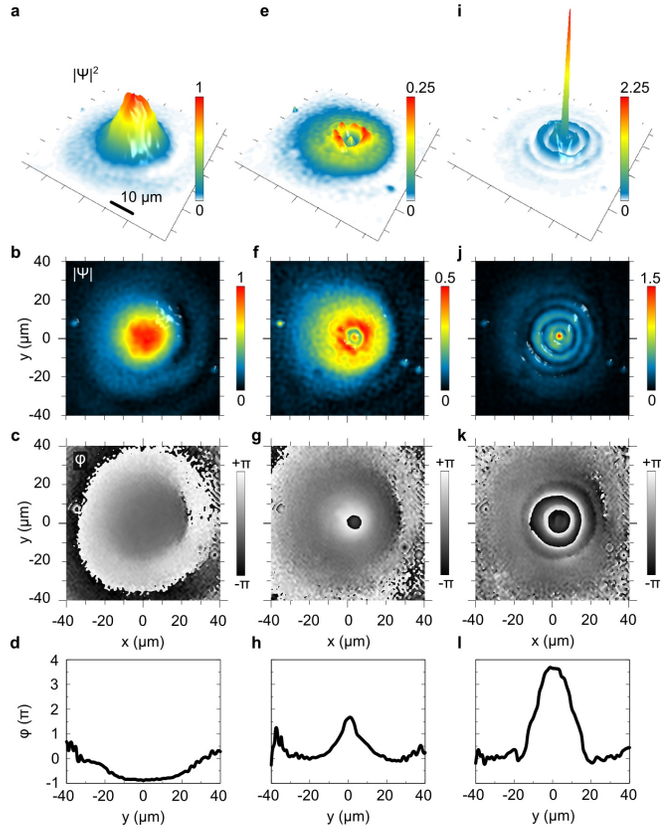

Figure 1: **Snapshots of the polariton fluid density and phase at three significative instants. a,e,i**, (first row) Density maps of the planar polariton condensate on a $80 \times 80\mu$m area as 3D view and **b,f,j** (second row) amplitude maps as 2D view. The three columns represent time frames at $t =$ 0 ps (a-d), 2.8 ps (e-h) and 10.4 ps (i-l). These time frames correspond respectively to the pulse arrival, the ignition of the dynamical peak and its long-lived state sitting at the center of a ring structure (see also video S1–S3). **c,g,k** (third row) phase maps and **d,h,l** (fourth row) unwrapped phase profiles along the radius. The phase gradient subtends the superflow and here exhibits a reversal of the phase curvature, leading to the development of an opposite flow, toward the center. The total number of particles intially excited in the whole area is 250×10^3 polaritons as evaluated by an independent measure of the bare emission.

Such an inversion in the phase gradient is an indication of a change in the fluid direction, from waves expanding outwards, to contracting towards the centre. This behaviour is then followed by the appearance of the bright and sharp central peak, contoured by concentric rings (i,j). This central peak collects 6% of the total particles still present in the fluid, and is surprisingly brighter than the initial spot was in the same area (here by a factor of two, up to ten times in other realizations, see supplementary Fig. S3) despite the total population having largely decreased (to less than 1/3 after 10 ps). Its localization goes below the resolution of our experimental setup and is thus less than 2 μm in width. The peak is furthermore extremely robust as it occurs over the whole sample area,

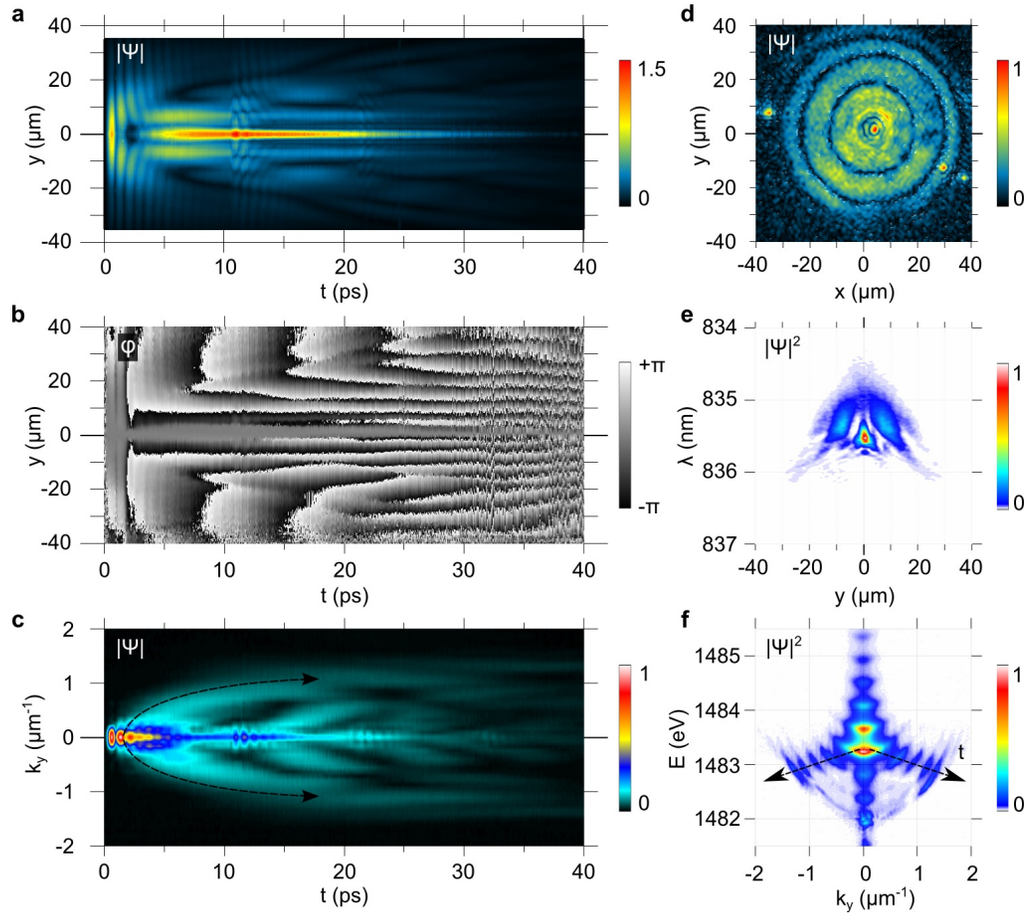

Figure 2: **Dynamical charts of the complex wavefunction and amplitude maps. a**, Time-space chart of the polariton amplitude $|\Psi(t,r)|$ sampled with a timestep $\delta t = 50$ fs. The polariton fluid oscillates with a Rabi period of about 800 fs (vertical stripes in the map), while the central density rapidly decays to zero before starting to rise as a bright peak. An echo pulse due to a reflection from the substrate edge is visible at $t = 11$ ps. **b**, Time-space chart of the phase $\Phi(t,y)$. Two diagonal horizon lines delimit an expanding region with large $\nabla\Phi$. **c**, The time evolution of amplitude in momentum space, $|\Psi(t,k_y)|$. The initial polariton population, featuring a very narrow Δk width (imparted by the photon packet), ejects an expanding disk developing into a ring. **d**, $|\Psi(x,y)|$ map at $t = 26$ ps, showing the dark/bright ring structures. **e**, A $y-\lambda$ cut showing the energy of the fluid along the diameter. The central brightest spot is less blueshifted than its sides. **f** Energy-momentum $E-k_y$ dispersion under the femtosecond coherent excitation. The dashed arrows depict the opening up in the k space and are associated to the dashed lines in panel **c**.

at different MC/QW detunings and even sustains motion, as it actually propagates if imparted with an initial momentum (see Supplementary Material). It is observed in the time-integrated camera images of the direct emission before any subsequent digital elaboration, which excludes any artifact of the technique (see also Fig. S3 in the Supplementary Material).

The full dynamics of the polariton fluid and the connection between the density accumulation and the radial flows are further studied in Fig. 2. Here are shown the amplitude and phase profiles versus time [panels (a) and (b)]. The amplitude chart reveals the bright peak as a central horizontal line which reaches its maximum intensity at a time of ∼11 ps. The vertical stripes observed in the first 5-6 ps are Rabi oscillations between the excitonic and photonic fields. The period of $T_R \approx 800$ fs corresponds to the energy separation between the UPB and LPB of 5.4 meV, while their fast decay is due to the rapid scattering of the UPB polaritons. The Rabi oscillations are triggered by the femtosecond pulse that excites simultaneously both polariton branches (9 nm energy width, see also supplementary Fig. S1 and Ref.[9]). They do not, however, play an important role in the observed phenomenology, since the dynamical localization also happens under the excitation of the LPB alone by a picosecond laser pulse (0.35 nm width, see supplementary Fig. S2). This confirms the robustness of this peak. Since it has an homogeneous phase, as can be seen from the phase graph in Fig. 2(b), it is a standing wave. We also note that a neat time-space cone marks a boundary between two regions: an expanding internal domain with almost horizontal black and white (b/w) bands (strong

inward $\nabla\Phi$) and an external domain with almost vertical b/w bands (null or weak $\nabla\Phi$). This is a clear evidence that a circular front of phase disturbance (marked also by a low density) is expanding ($\sim 1\mu$m/ps), leaving after its passage a fragmentation into multiple rings, as illustrated in the still image of panel (d). If an attractive term is at play here, it thus seems to be in the course of expanding its range of action. To further characterize the flow dynamics and its role in the formation of the central peak, we extend our study to the reciprocal space, reporting the 1D cross section of the k_x, k_y plane in panel (c) of figure 2. The initial Δk width of the polariton population created by the laser pulse is very small ($\sim 0.24\mu m^{-1}$ FWHM) and concentrated around $k = 0$. After a couple of picoseconds, the fluid suddenly ejects a disk in k-space which stabilizes within 10 ps into a ring at finite momenta around $|k| = 1\mu m^{-1}$. These are clearly associated to the inner growing flow. Looking at the onset of the Rabi oscillations allows us to make a correspondence between real and reciprocal space, indicating that the central bright peak in real space is associated to the finite momenta travelling waves in reciprocal space. The energy of these waves is shown in the integrated dispersion of Fig. 2(f)[33]. Note that, as oberved in the dispersion plotted in Fig. 2(f), the ring in k space gradually expands from $k = 0$ at early times (maximum blushift of the polariton pupulation) to the value of $|k| = 1.25\mu m^{-1}$ when the dispersion is redshifted to its original bare energy. The space-energy profile in figure 2(e) explains in part the inner flow. Here it is clear that the central part of the spot is redshifted with respect to the sides, hinting at the presence of an effective attractive potential responsible for the central peak of high polariton density. Although it is not clear at the outset what the origin of such a potential is, it is consistent with an attractive term (nonlinearity inversion) or with nonlocal interactions, i.e., k-dependent blueshift[5,34]. In our case, we may reasonably infer that the inward coherent waves generated by such a potential interfere in the center with opposite k_r vectors, explaining the central accumulation enhanced by a polar scaling of $1/r$ which is typical of an interfering ring wave (see figure S7 in the SM).

To verify the nature of the interference, we report the phase and amplitude profiles at different time stills. In Fig. 3(a), the phase profile during the first 5 ps is shown. Soon after the phase reversal, a sudden, almost instantaneous switch happens at $t = 1.5$ ps. The rigid switch is a π-jump, corresponding to the dark notch in the density, as seen in panel (b). This is a typical sign of an interference between counterpropagating waves. In the following dynamics, as already said, the reversed gradient tends to grow and expand all over the originally excited area, as depicted in panel (c) with profiles at 5 ps intervals. Other π-jumps in the phase can be observed at a later time, corresponding to dark rings in the density, see Fig. 3(d). This is an evidence that interference phenomena of coherent waves are acting in reshaping the fluid density as a series of concentric rings. It also suggests

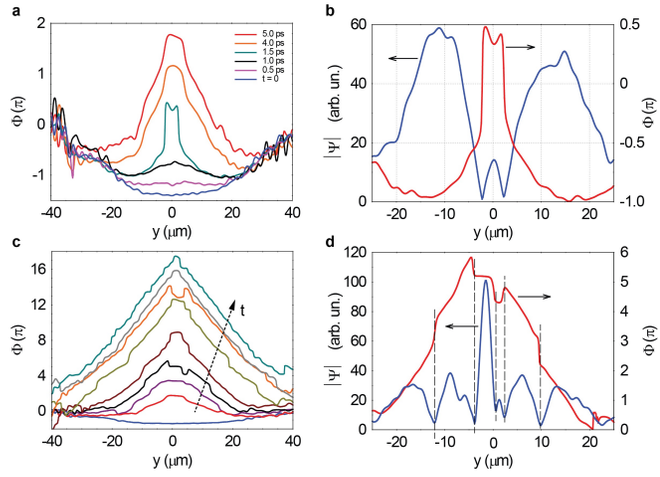

Figure 3: **Phase crosscuts during the fluid evolution and signature of dark ring solitons. a**, Unwrapped radial phase profile at early time, showing the reversal of the phase curvature. **b**, The sudden phase switch at $t = 1.5$ ps is shown together with the associated amplitude profile. The dip in the intensity with the π-jump in phase is a signature of radial interference and of a possible dark ring soliton, surrounding the bright peak. **c**, Radial phase profile at later time, taken each 5 ps over a 0–40 ps timespan. The phase slope increases with time up to $\nabla\phi \sim 2\pi/5\mu m \simeq 1.25\mu m^{-1}$. **d**, Amplitude and phase profiles at 16 ps showing that a nonlinear interference is reshaping the fluid in a series of concentric rings.

a possible link to—without being a "per-se" proof of—ring dark solitons (RDS)[35]. These specific solutions to nonlinear Schrödinger equations (NLSE) under repulsive interactions are predicted to become stable in the case of 2D fluids such as polaritons[36]. It appears that a RDS indeed holds for the first dark ring around the rising bright peak, given its stability for several tens of ps.

The nonlinear nature of the effect is demonstrated in Fig. 4. At low density, Fig. 4(a,b,c), the condensate behaves as expected from any fluid freely released, with a small diffusion and remaining homogeneous in both density and phase, as well as, in our case, Rabi oscillations at earlier times. It is also clear that the expansion speed imparted by the small initial Δk is negligible. At 5-times higher excitation power [Fig. 4(d,e,f)], there is a density redistribution of polaritons to form the central localization peak, surrounded by ring structures and out-radiating shock waves, however, yet without a strong enhancement and a moderate phase reversal. In Fig.4(g,h,i), at 18 times the initial pumping power, the structure gets fully formed, with a central peak gathering over twice the population locally present at the initial time and with a much steeper phase reversal, giving rise to the striking structure in Fig. 4h. Here again we emphasize that the central peak is resolution limited and is likely sharper than is resolved in our experiment. Additional examples are provided in the supplementary Fig. S3 for an extended set of excitation densities.

We now discuss which physical mechanism could be

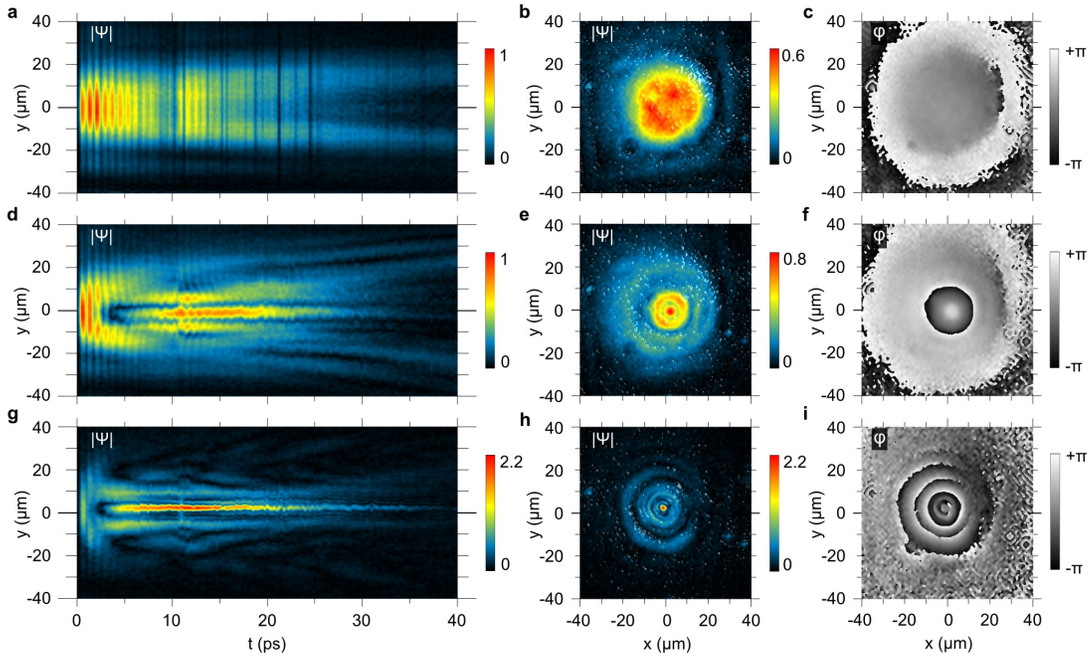

Figure 4: **Time-space charts and space maps for different density regimes of excitation.** Time evolution of the radial modulus $|\Psi(t, y)|$ for three different powers (**a,d,g**, left column), and relative amplitude $|\Psi(x, y)|$ (**b,e,h**) and phase $\Phi(x, y)$ (**c,f,i**) maps at $t = 12$ ps (mid and right columns, respectively). Increasing the initial density leads to a faster central depletion and stronger rise-back reaction. In the third row the dominating feature is the bright peak, with an enhancement factor of almost 5 in intensity, while outradiated waves are faster but almost canceled out on a relative scale. This demonstrates the strong nonlinearities acting in the central gathering of polaritons and in setting the radial k and speed of the ring waves. The three rows refer to initial total populations (top density) of 25×10^3 ($55\mu m^{-2}$), 125×10^3 ($275\mu m^{-2}$) and 450×10^3 polaritons ($1000\mu m^{-2}$), respectively.

responsible for such a remarkable phenomenology. The strong-coupling regime of light and matter at the core of the polariton physics can lead to distinctive dispersive and dissipative nonlinearities[6,37–39]. For instance, polaritons support dissipative solitons[40], have demonstrated bistability domains with a switching on/off of both bright and dark solitons[41] as well as moving bright solitons along a steadily pumped background[8,15] (this last based on the negative curvature of the polariton dispersion above the inflexion point). All these features are accountable by one of the several models used to describe polariton fluids. While the positive nonlinearities intrinsic to polariton interactions, due to the excitonic repulsions, are supposedly able to force the expansion and reshaping of a polariton fluid and to sustain dark solitons[35], possibly shedding light to some aspect of our experiment, there is no documented mechanism to explain the most striking feature: the real-space collapse in the center of the spot. Real space localization could in principle appear under negative, i.e., attractive, nonlinearities[6]. As we review below all the obvious candidates to account for the observed phenomenology, we can rule out this and other tempting explanations. Our analysis will show that the most likely origin of the nonlinear activation of a central bright spot is the self-trapping of a polariton condensate by a type of collective polaron effect.

A first possibility to explain the self-localization is for the polariton population at early times to undergo a transition to the weak coupling regime (screening and reduction of coupling). Although this can be partially happening at the largest power (given the excited density there is $0.33 \times 10^3 \mu m^{-2}$ per QW and approaches values of the so-called Mott density, in the order of $2 \div 5 \times 10^3 \mu m^{-2}$), it does not explain the effect since (i) the blueshift of the LPB is continuous and does not reach the photonic mode; (ii) increasing power/density does not increase the size of the bright peak, as expected if merely enlarging the size of an above-threshold region; (iii) the total intensity decays with the LP polariton lifetime of 10 ps (see supplementary Fig. S1) and (iv) transition to weak coupling for excitation below the band edge would manifest as a higher blueshift as follows from the nonlinear Kramers-Kronig relations[42,43], while we observe a lesser blueshift in the centre with respect to the side bright ring, as shown in Fig. 2(e). An exciton reservoir, separate from the polariton condensate, is known to play a significant role in many polariton experiments. We can exclude it in our case for the following reasons: (i) the effect persists when resonantly exciting the lower polariton branch, a configuration that does not populate the reservoir (see the supplementary Fig. S2 on the picosecond experiment), (ii) a moving bright peak is observed

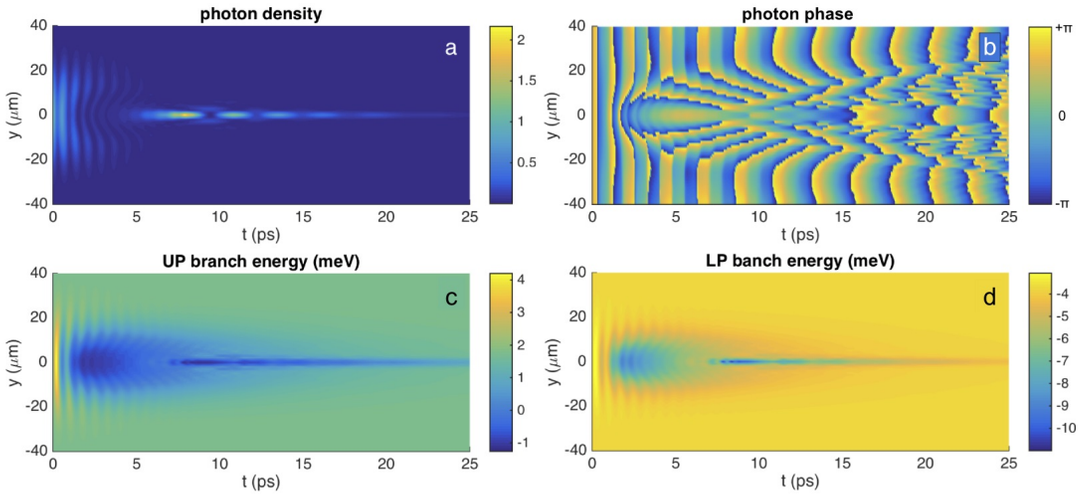

Figure 5: The calculated magnitude of the polariton condensate as a function of y-coordinate and time (a) together with its phase (b). The corresponding calculated energy profiles for the upper and lower polariton branches are shown in panels (c) and (d), respectively.

when exciting with nonzero initial in-plane wavevector k, ruling out a reservoir that would need to be dragged by the structure as it propagates, which is impossible given the heavy mass of the reservoir excitons (see the supplementary Fig. S6 on the moving peak), (iii) the effect does not show any strong polarization dependence. These considerations thus exclude the case of a dissipative bright soliton[40] predicted under cw pumping where the localization is sculpted by an interplay between source and decay regions and the compensation of their steady flows. The appealing recourse to attractive interactions cannot be sustained either. While polariton attractions are possible due to the various superexchange processes through dark excitons or bi-exciton states, or due to Van der Waals forces, none of these mechanisms can account for the experiment in a careful analysis. The former mechanism should be strongly polarisation dependent[6,37], which is not our case, and the latter are too small with respect to the repulsive Coulomb or exchange terms[6]. Similarly, nonlocality (k-dependence, which could also lead to a negative dispersion in the centre of the spot[34]) of one or more of these terms and even retardation effects are negligible as well[5] and fail to produce the real-space collapse in numerical simulations. Intriguingly, the dynamical Casimir effect[44] recently proposed[45] in a configuration very similar to our experiments, was predicted to generate finite momentum excitations from the vacuum adding up to the suddenly excited fluid at $k = 0$. However, this effect, was considered only for the homogeneous 1D polariton at zero temperature, and the model is not ready to be compared at its stage of development with the configuration of our experiment.

The failures of these analyses point at an unconventional mechanism ruling the high-density, ultrafast dynamics of polaritons. Given that the object appears to be self-sustained, it is important to elucidate its nature, as it may have important applications, especially as the control of ultra-sharp localized light peaks is clearly of technological interest, for instance for high-resolution displays or memory units. One of the unconventional scenarios that we found to be fairly consistent with most the hypotheses and observations of our experiment involves a sort of collective polaron effect. The recent work by Klembt *et al.*[46] shows that the resonant pumping of exciton polaritons into a microcavity may result both in cooling or heating of the crystal lattice depending on the initial lattice temperature and the optical pump power. In our experiments, realised at a cryogenic temperature and sufficiently high pump power, one should expect such a local heating of the crystal lattice due to the polariton Auger process, followed by the emission of a cascade of acoustic phonons. The probability of this process is quadratic in the polariton density. The heating results in the local band-gap renormalisation which is responsible for the red-shift of the exciton energy. The heating by 20-30 degrees results in a redshift of the exciton energy of 1-2 meV, which is sufficient for trapping the polariton condensate. In this way, a trap in real space is formed under the pump spot. It becomes deeper as more polaritons are getting trapped, thus providing a positive feedback that stabilizes the self-trapping process and explain the robustness of the effect. We have modeled this mechanism through a generalised Gross-Pitaevskii equation, described in the Supplementary Material. Figure 5 shows a result of the numerical simulation for the wavefunction of the polariton condensate ruled by this process. The upper panel shows the real-space dynamics and next panels the energies of the low and upper polariton branches, respectively. Beyond the dynamics of the Rabi oscillations, in particular their bending, the model also reproduces the self-localization in good qualitative agreement with the experimental data.

In conclusions, we have observed the dynamical appearance of a bright and sharp peak sitting at the center of a series of concentric rings in a polariton fluid generated by the sudden excitation from a resonant laser pulse at $k = 0$. The peak that appears at high pumping is robust to other variations in the experimental parameters (detuning, momentum, etc.), is resolution limited and gathers up to ten times the population initially present in its area. This striking structure cannot be explained by any of the conventional mechanisms such as loss of strong-coupling nor by the common models of polariton dynamics, including Gross-Pitaevskii type of equations with or without reservoirs and/or attractive interactions. We have provided a possible intepretation in terms of the collective polaron effect, resulting in a self-trapping of the polariton condensate. Our results show that much is left to explore in the high-density and ultrafast dynamics of polaritons, with a striking and unique phenomenology that could open new areas of research and applications.

Acknowledgments

We acknowledge R. Houdré for the growth of the microcavity sample and the project ERC POLAFLOW for financial support. This work has been partially funded by the Quandyde project of the ANR France and by the CLERMONT4 Network Program. MM acknowledges support from the National Science Center grant DEC-2011/01/D/ST3/00482.

[1] Amo, A. *et al.* Collective fluid dynamics of a polariton condensate in a semiconductor microcavity. *Nature* **457**, 291–5 (2009). http://dx.doi.org/10.1038/nature07640.

[2] Kasprzak, J. *et al.* Bose-Einstein condensation of exciton polaritons. *Nature* **443**, 409–14 (2006). http://dx.doi.org/10.1038/nature05131.

[3] Amo, A. *et al.* Superfluidity of polaritons in semiconductor microcavities. *Nature Physics* **5**, 805–810 (2009). http://dx.doi.org/10.1038/nphys1364.

[4] Nardin, G. *et al.* Hydrodynamic nucleation of quantized vortex pairs in a polariton quantum fluid. *Nature Physics* **7**, 635–641 (2011). http://dx.doi.org/10.1038/nphys1959.

[5] Luk, M. H. *et al.* Transverse optical instability patterns in semiconductor microcavities: Polariton scattering and low-intensity all-optical switching. *Phys. Rev. B* **87**, 205307 (2013). http://link.aps.org/doi/10.1103/PhysRevB.87.205307.

[6] Vladimirova, M. *et al.* Polariton-polariton interaction constants in microcavities. *Phys. Rev. B* **82**, 075301 (2010). http://link.aps.org/doi/10.1103/PhysRevB.82.075301.

[7] Carusotto, I. & Ciuti, C. Quantum fluids of light. *Rev. Mod. Phys.* **85**, 299–366 (2013). http://link.aps.org/doi/10.1103/RevModPhys.85.299.

[8] Sich, M. *et al.* Observation of bright polariton solitons in a semiconductor microcavity. *Nature Photonics* **6**, 50–55 (2012). http://dx.doi.org/10.1038/nphoton.2011.267.

[9] Dominici, L. *et al.* Ultrafast control and rabi oscillations of polaritons. *Phys. Rev. Lett.* **113**, 226401 (2014). doi:10.1103/PhysRevLett.113.226401.

[10] Ballarini, D. *et al.* All-optical polariton transistor. *Nature Communications* **4**, 1778 (2013). http://www.ncbi.nlm.nih.gov/pubmed/23653190.

[11] Sanvitto, D. *et al.* Persistent currents and quantized vortices in a polariton superfluid. *Nature Physics* **6**, 527–533 (2010). http://www.nature.com/doifinder/10.1038/nphys1668.

[12] Manni, F., Léger, Y., Rubo, Y. G., André, R. & Deveaud, B. Hyperbolic spin vortices and textures in exciton-polariton condensates. *Nature Communications* **4** (2013). http://www.nature.com/ncomms/2013/131009/ncomms3590/abs/ncomms3590.html?message-global=remove.

[13] Grosso, G., Nardin, G., Morier-Genoud, F., Léger, Y. & Deveaud-Plédran, B. Dynamics of dark-soliton formation in a polariton quantum fluid. *Physical Review B* **86**, 020509 (2012). http://link.aps.org/doi/10.1103/PhysRevB.86.020509.

[14] Pigeon, S., Carusotto, I. & Ciuti, C. Hydrodynamic nucleation of vortices and solitons in a resonantly excited polariton superfluid. *Physical Review B* **83**, 144513 (2011). http://link.aps.org/doi/10.1103/PhysRevB.83.144513.

[15] Sich, M. *et al.* Effects of spin-dependent interactions on polarization of bright polariton solitons. *Phys. Rev. Lett.* **112**, 046403 (2014). http://link.aps.org/doi/10.1103/PhysRevLett.112.046403.

[16] Tanese, D. *et al.* Polariton condensation in solitonic gap states in a one-dimensional periodic potential. *Nature Communications* **4**, 1749 (2013). http://dx.doi.org/10.1038/ncomms2760.

[17] Zhang, W. L. & Yu, S. F. Vectorial polariton solitons in semiconductor microcavities. *Optics Express* **18**, 21219–24 (2010). http://www.opticsexpress.org/abstract.cfm?URI=oe-18-20-21219.

[18] Ghofraniha, N., Gentilini, S., Folli, V., Del Re, E. & Conti, C. Shock Waves in Disordered Media. *Physical Review Letters* **109**, 243902 (2012). http://link.aps.org/doi/10.1103/PhysRevLett.109.243902.

[19] Wan, W., Jia, S. & Fleischer, J. W. Dispersive superfluid-like shock waves in nonlinear optics. *Nature Physics* **3**, 46–51 (2006). http://dx.doi.org/10.1038/nphys486.

[20] Chang, J., Engels, P. & Hoefer, M. Formation of Dispersive Shock Waves by Merging and Splitting Bose-Einstein Condensates. *Physical Review Letters* **101**, 170404 (2008). http://link.aps.org/doi/10.1103/PhysRevLett.101.170404.

[21] Dutton, Z., Budde, M., Slowe, C. & Hau, L. V. Observation of Quantum Shock Waves Created with Ultra- Compressed Slow Light Pulses in a Bose-Einstein Condensate. *Science* **293**, 663–668 (2001). http://www.sciencemag.

org/content/293/5530/663.abstract.

[22] Eiermann, B. *et al.* Bright Bose-Einstein Gap Solitons of Atoms with Repulsive Interaction. *Physical Review Letters* **92**, 230401 (2004). http://link.aps.org/doi/10.1103/PhysRevLett.92.230401.

[23] Hai, W., Zhu, Q. & Rong, S. Chaotic shock waves of a Bose-Einstein condensate. *Physical Review A* **79**, 023603 (2009). http://link.aps.org/doi/10.1103/PhysRevA.79.023603.

[24] Joseph, J. A., Thomas, J. E., Kulkarni, M. & Abanov, A. G. Observation of Shock Waves in a Strongly Interacting Fermi Gas. *Physical Review Letters* **106**, 150401 (2011). http://link.aps.org/doi/10.1103/PhysRevLett.106.150401.

[25] Kamchatnov, A., Gammal, A. & Kraenkel, R. Dissipationless shock waves in Bose-Einstein condensates with repulsive interaction between atoms. *Physical Review A* **69**, 063605 (2004). http://link.aps.org/doi/10.1103/PhysRevA.69.063605.

[26] Marchant, A. L. *et al.* Controlled formation and reflection of a bright solitary matter-wave. *Nature Communications* **4**, 1865 (2013). http://dx.doi.org/10.1038/ncomms2893.

[27] Simula, T. *et al.* Observations on Sound Propagation in Rapidly Rotating Bose-Einstein Condensates. *Physical Review Letters* **94**, 080404 (2005). http://link.aps.org/doi/10.1103/PhysRevLett.94.080404.

[28] Barland, S. *et al.* Cavity solitons as pixels in semiconductor microcavities. *Nature* **419**, 699–702 (2002). http://dx.doi.org/10.1038/nature01049.

[29] Barland, S. *et al.* Solitons in semiconductor microcavities. *Nature Photonics* **6**, 204–204 (2012). http://dx.doi.org/10.1038/nphoton.2012.50.

[30] Barsi, C., Wan, W., Sun, C. & Fleischer, J. W. Dispersive shock waves with nonlocal nonlinearity. *Optics Letters* **32**, 2930 (2007). http://ol.osa.org/abstract.cfm?URI=ol-32-20-2930.

[31] Antón, C. *et al.* Role of supercurrents on vortices formation in polariton condensates. *Optics Express* **20**, 16366 (2012). http://www.opticsexpress.org/abstract.cfm?URI=oe-20-15-16366.

[32] Schnars, U. & Jüptner, W. *Digital Holography* (Springer Berlin Heidelberg, 2005).

[33] Please note that the apparent discretization in energy is given by the interference in the energy domain of time-delayed reflections back from the substrate edge and is not affecting the ongoing dynamics; the substrate has got a 1.5 mm optical thickness, associated to a 10 ps time distance of the reflected echos of the emission and to a 0.45 mev fringes spacing in energy; the emission echo is visible also in the time-space measurements of real and reciprocal space, where it is seen weaker and weaker at regular interval of 10 ps.

[34] Baumberg, J. J. & Lagoudakis, P. G. Parametric amplification and polariton liquids in semiconductor microcavities. *Physica Status Solidi (b)* **242**, 2210–2223 (2005). http://dx.doi.org/10.1002/pssb.200560960.

[35] Kivshar, Y. & Yang, X. Ring dark solitons. *Physical Review E* **50**, R40–R43 (1994). http://journals.aps.org/pre/abstract/10.1103/PhysRevE.50.R40.

[36] Rodrigues, A. S. *et al.* From nodeless clouds and vortices to gray ring solitons and symmetry-broken states in two-dimensional polariton condensates. *Journal of Physics: Condensed Matter* **26**, 155801 (2014). http://stacks.iop.org/0953-8984/26/i=15/a=155801.

[37] Takemura, N., Trebaol, S., Wouters, M., Portella-Oberli, M. T. & Deveaud, B. Polaritonic Feshbach resonance. *Nature Physics* **10**, 500–504 (2014). http://dx.doi.org/10.1038/nphys2999.

[38] Weiss, C. O. & Larionova, Y. Pattern formation in optical resonators. *Reports on Progress in Physics* **70**, 255 (2007). http://stacks.iop.org/0034-4885/70/i=2/a=R03.

[39] Schaefer, A. C. & Steel, D. G. Nonlinear optical response of the gaas exciton polariton. *Phys. Rev. Lett.* **79**, 4870–4873 (1997). http://link.aps.org/doi/10.1103/PhysRevLett.79.4870.

[40] Ostrovskaya, E. A., Abdullaev, J., Desyatnikov, A. S., Fraser, M. D. & Kivshar, Y. S. Dissipative solitons and vortices in polariton Bose-Einstein condensates. *Physical Review A* **86**, 013636 (2012). http://link.aps.org/doi/10.1103/PhysRevA.86.013636.

[41] Larionova, Y., Stolz, W. & Weiss, C. O. Optical bistability and spatial resonator solitons based on exciton-polariton nonlinearity. *Optics Letters* **33**, 321 (2008). http://ol.osa.org/abstract.cfm?URI=ol-33-4-321.

[42] Garmire, E. Resonant optical nonlinearities in semiconductors. *Selected Topics in Quantum Electronics, IEEE Journal of* **6**, 1094–1110 (2000).

[43] Taranenko, V., Slekys, G. & Weiss, C. Spatial resonator solitons. In Akhmediev, N. & Ankiewicz, A. (eds.) *Dissipative Solitons*, vol. 661 of *Lecture Notes in Physics*, 131–160 (Springer Berlin Heidelberg, 2005). http://dx.doi.org/10.1007/10928028_6.

[44] Zhang, X., Yang, H., Zheng, T. & Pan, S. Linking the dynamical casimir effect to the collective excitation effect at finite temperature. *International Journal of Theoretical Physics* **53**, 510–518 (2014). http://dx.doi.org/10.1007/s10773-013-1834-6.

[45] Koghee, S. & Wouters, M. Dynamical casimir emission from polariton condensates. *Phys. Rev. Lett.* **112**, 036406 (2014). http://link.aps.org/doi/10.1103/PhysRevLett.112.036406.

[46] Klembt, S. *et al.* Exciton-polariton gas as a nonequilibrium coolant. *Phys. Rev. Lett.* **114**, 186403 (2015). http://link.aps.org/doi/10.1103/PhysRevLett.114.186403.

Supplementary Material

In this Supplementary Material, we describe the supplementary movies, some supporting experimental figures and discuss several theoretical models used in attempt to describe the collapse in real space of the polariton condensate.

Supporting experimental figures S1-S7

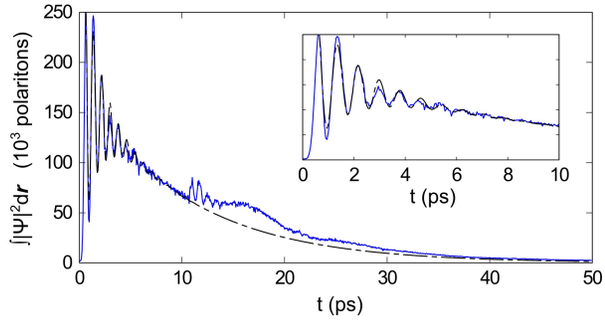

Figure S1: Total intensity versus time in the femtosecond experiment of Fig. 1-3 of the main text. Blue line are the experimental data of the area-integrated emission intensity sampled every 50 fs. The black line is a fit based on a model of coupled and damped oscillators. The inset is an enlargement of the first 10 ps.

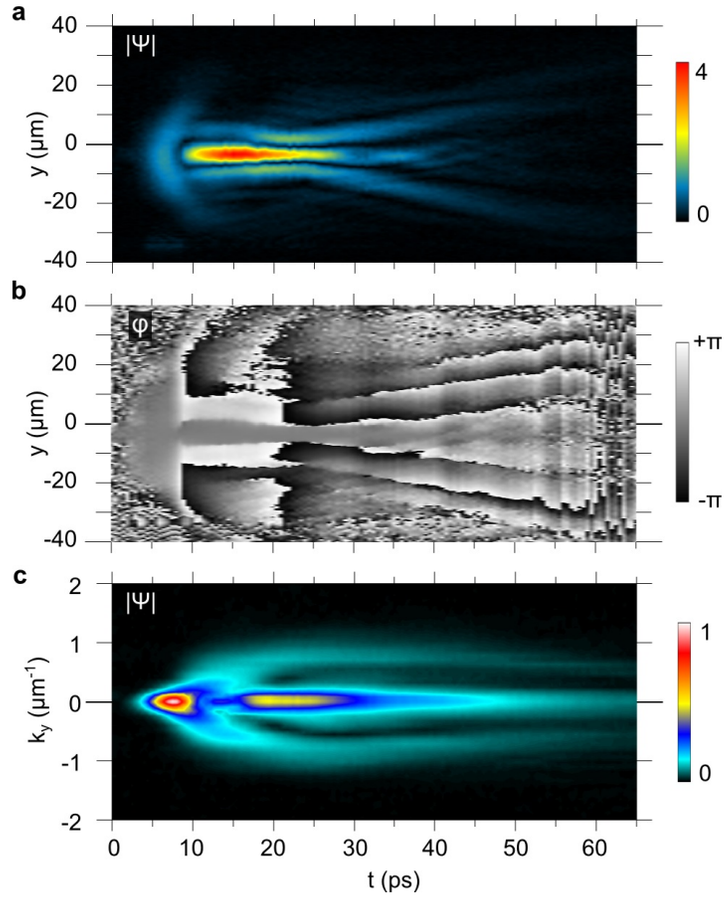

Figure S2: Picosecond experiment. The excitation pulse is a 3.5 ps width laser pulse resonant on the LPB. The three panels show the time-space graphs of the amplitude (a), phase (b) and k-space (c) cross cuts with a time step of 0.5 ps. The LUT colour scale in the case of the amplitude chart in (a) is relative to the initial top amplitude, and represents an enhancement factor of 4 at around 10 ps after the pulse arrival, which corresponds to a factor of 16 in density.

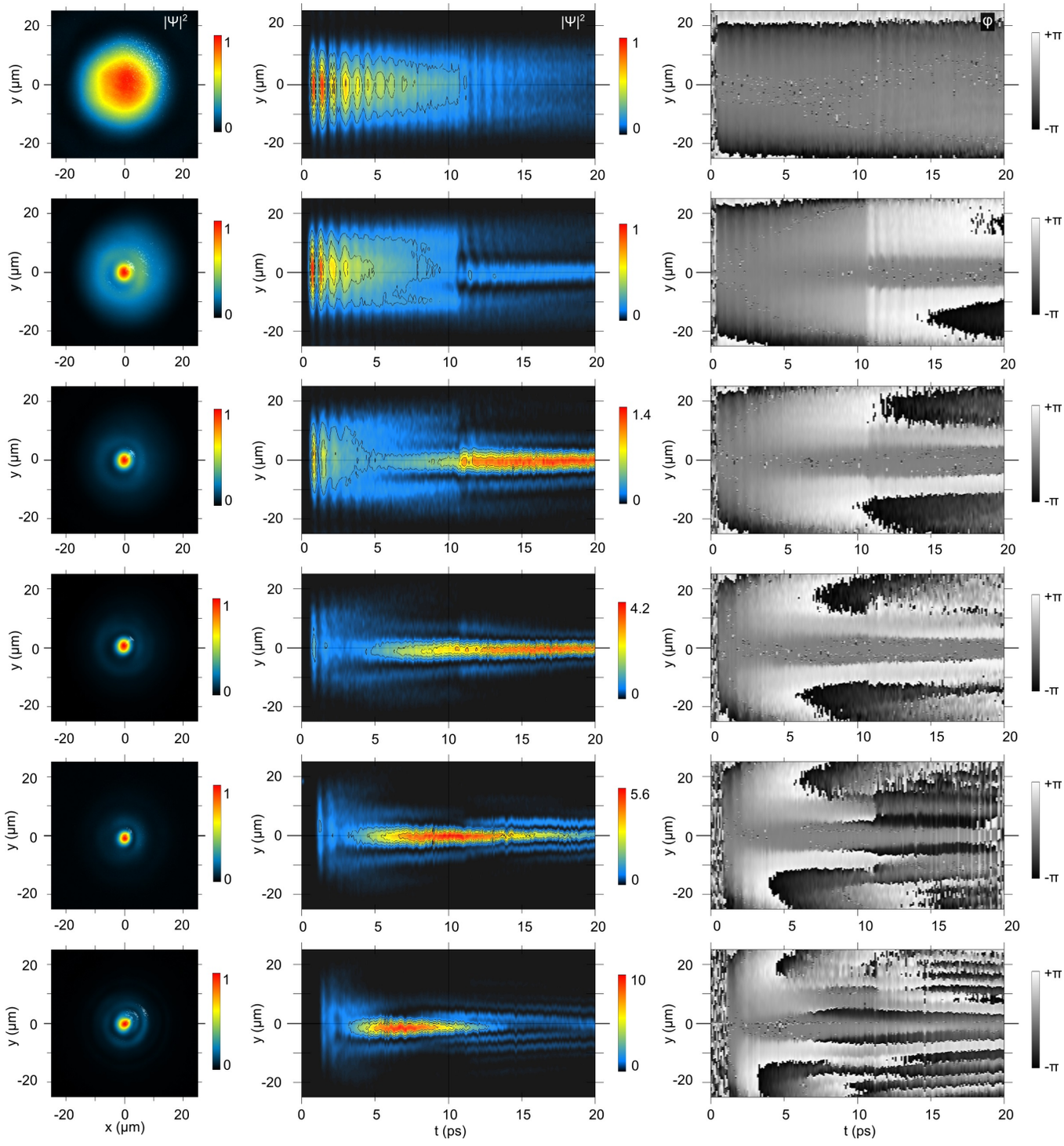

Figure S3: Femtosecond experiment at several excitation powers with a $16\mu m$ FWHM gaussian spot and linear polarization. Each row is relative to a different initial density. The first column represents the time-integrated images of the bare emission in space directly aquired on the camera. The second and third columns represent the density and phase profiles, respectively, along a central diameter and versus time, retrieved by means of the ultrafast imaging. The powers are increasing from top to bottom rows and are relative to initial total populations of P_1–P_6 = 100×10^3, 200×10^3, 350×10^3, 550×10^3, 1×10^6 and 2.1×10^6 polaritons. The corresponding initial top densities are: 345 μm^{-2}, 790 μm^{-2}, $1200\mu m^{-2}$, $1900\mu m^{-2}$, $3450\mu m^{-2}$ and $7200\mu m^{-2}$, respectively. The maxima on the colour bars of the density charts are expressed in terms of the initial top densities and represent the achieved enhancement factors. From the blueshift associated to P_5, we evaluated a nonlinearity $g \sim 0.001 meV\mu m^2$ to be renormalized to $g \sim 0.003 meV\mu m^2$ for a single QW.

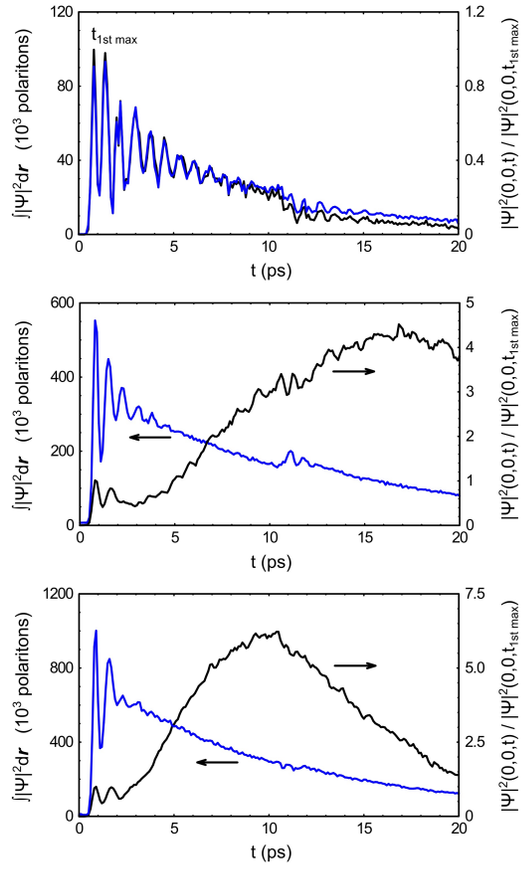

Figure S4: Total and central density in the case of the femtosecond experiments of the previous figure S3, for the excitation powers P_1, P_4 and P_5 as a function of time. The blue curve plotted on the left gives the total number of polaritons with time while the black curve plotted on the right gives the corresponding density in the centre as a ratio with respect to the one at the time of the first peak.

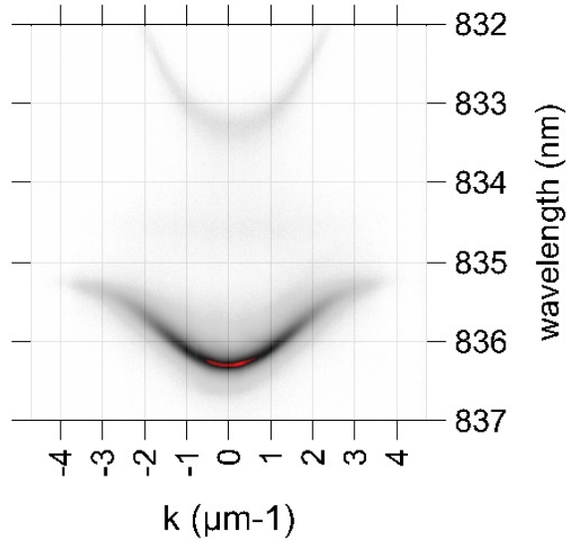

Figure S5: Polariton dispersion. The bare E–k emission of the microcavity polaritons is obtained after offresonant cw excitation at low power. The separation of the UPB and LPB branches is 5.4 meV/3 nm.

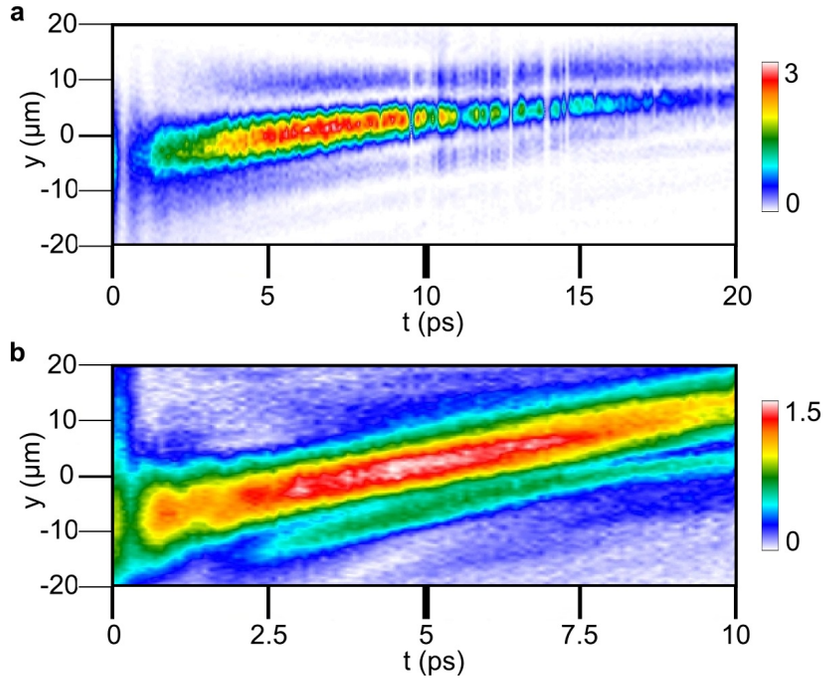

Figure S6: Propagating bright peak activated under resonant fs pulse injection with (a) $0.7\mu m^{-1}$ and (b) $1.6\mu m^{-1}$ in-plane wavevectors k_y. The cuts of the spatial polariton density as a function of time are taken along the propagation direction.

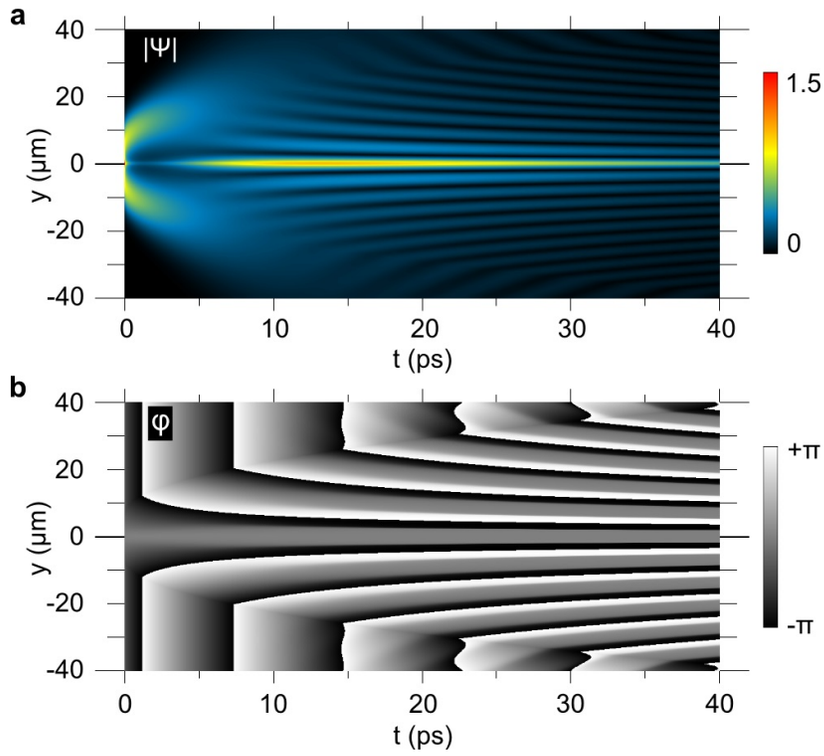

Figure S7: Interferometric model from a ring source. The ring corresponds to a double gaussian along a diameter cross-cut. The ring radius and width are let to expand in time, which correspond to the two gaussians moving and expanding, respectively. The phase is modulated by a radial in-plane wavevector which slightly increases in time. The part of the ring which reaches the centre emerges on the other side and interferes with the opposing wavevector fluid, causing a structure similar to that observed in the experiment.

Theoretical models

The model commonly used to describe the dynamics of polaritons is based on the mean-field approach. The time evolution of the photonic (excitonic) wavefunctions $\phi(\mathbf{r})$ ($\chi(\mathbf{r})$) is given by coupled Gross-Pitaevskii equations[S1,S2]:

$$\begin{aligned} i\hbar\frac{\partial\phi}{\partial t} &= (E_C - \frac{\hbar^2}{2m_C}\nabla^2)\phi + \frac{\hbar\Omega_R}{2}\chi - \frac{i\hbar}{2\tau_C}\phi + F_p(\mathbf{r},t), \\ i\hbar\frac{\partial\chi}{\partial t} &= (E_X - \frac{\hbar^2}{2m_X}\nabla^2)\chi + \frac{\hbar\Omega_R}{2}\phi + g|\chi|^2\chi, \end{aligned} \tag{S1}$$

where m_C (m_X) is the cavity photon (exciton) effective mass, g is the exciton-exciton interaction constant, Ω_R is the Rabi frequency determining the exciton-photon coupling, $F_p(\mathbf{r},t) = F_0 e^{-\mathbf{r}^2/2W^2 - t^2/2T_p^2 - iE_p t}$ is the pumping field describing the pulsed excitation of the cavity with a Gaussian spot of diameter $2W$ and pulse-duration of $2T_p$ and F_0 is a parameter determining the density of photo-created carriers. While this model has been successful to describe much of the fluid dynamics of polaritons, including ballistic motion[S3,S4], superfluidity[S5], solitons[S6], etc.[S7], in presence of repulsive interactions, $g > 0$, it cannot account for real-space localization. Many additional ingredients to these equations can produce qualitatively the most important feature of our experiment, the formation of a high density peak in the center. However, these extended models, based on different physical assumptions, have some implications, present other qualitative features and/or require certain ranges or parameters that rule them out as an explanation of the phenomenon. Some hypotheses that work reasonably well demand assumptions that are difficult to justify, such as explicit attractive interactions, $g < 0$. We found that one model only is sufficiently consistent with all the observations and provides a reasonably close agreement with the data to be retained as a possible mechanism for our experiment. It is presented last in a series of alternative descriptions, below: the loss of strong coupling in Section I, a localisation due to the exciton reservoir or dark excitons in Section II, polaritons with attractive interactions in Section III—all of these models failing in some fatal way to account for the experiment—and, ultimately, the collective polaron effect, in Section IV, which, on the contrary, reproduces adequately the findings, based on likely assumptions and parameters corresponding to our sample.

I. LOSS OF STRONG-COUPLING

The measured emission of total emitted photons from a single experiment suggests that the exciton density is close to the saturation value of $n_{\text{sat}} \approx 10^3 \mu m^{-2}$. At such a high density, the reduction of the Rabi splitting should occur due to phase space filling[S1,S8–S11] and lead to a modification of the polariton dispersion. At the first order of perturbation in the exciton density, the saturation is momentum-independent, or local in space (precisely, the range of the interaction is of the order of the exciton radius)[S9–S11]. The linear regime Rabi coupling Ω_{R0} is then renormalized to:

$$\Omega_R = \Omega_{R0} - a\frac{g|\chi|^2}{\hbar} \tag{S2}$$

where a is the coefficient dependent on the quantum well geometry, g the polariton-polariton interaction strength and χ the exciton wavefunction (as already defined before). This leads to effective attractive interactions but only for the UP branch, while the interactions remain repulsive for the LP branch[S1]. This is because the UP branch is redshifted whilst the Rabi coupling decreases, while the LP branch is blueshifted, just as it would be from repulsive interactions. A numerical simulation for this mechanism is shown in Fig. S8. This model correctly reproduces the experimental Rabi bending and allows to describe a central density peak with both a femtosecond pulse and a picosecond pulse tuned to the UP branch. Critically, however, the ps pulse excitation tuned to the LP branch leads to strong defocusing in this model, in contradiction with the experimental data.

To overcome the defocusing in the case of LP branch excitation, we can consider a momentum-dependent loss of the Rabi coupling. Assuming a stronger reduction of Ω_R in the vicinity of $k = 0$, where lies the condensate whose density is responsible for the phase-space filling, allows to create a negative effective mass for the lower polariton. Indeed, the LP polariton branch blueshifts more at $k = 0$, creating a negative curvature of the dispersion around the ground state, allowing for self-focusing even with repulsive interactions. Technically, this can be achieved by filtering Eq. (S2) in k space. In the simplest formulation, this is done by transforming the excitonic wavefunction $\phi = |\chi|^2\psi$ to k-space, applying a Gaussian filter $\phi_1(k) = \phi(k)\exp(-k^2/2k_c^2)$, transforming it back, and subtracting from the Ω_{R0} term after multiplication by $ag/\hbar$. This nonlocal and nonlinear reduction of the Rabi coupling is equivalent to introducing interactions that are nonlocal in real space. The range of the nonlocal effective interaction is given by

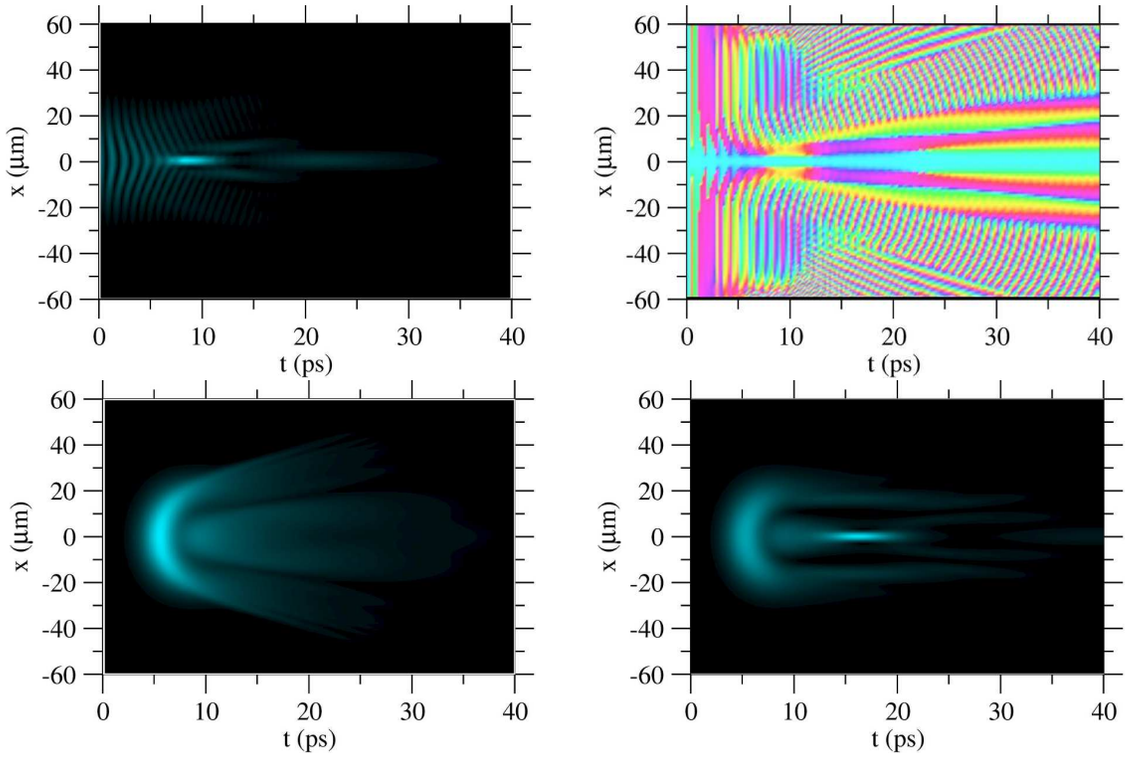

Figure S8: Evolution of the photon field intensity in the model with density dependent reduction of the Rabi coupling. Top frames show the photon field density and phase, respectively, in the case of femtosecond pulse excitation. Bottom frames show picosecond pulse excitation at the position of the UP branch (left), featuring a real-space localization, and at the position of the LP branch (right), failing to produce the localization. Parameters are $\Omega_R = 2\pi/(0.8\text{ps}) - (3/2\hbar)g|\chi|^2$, $\delta = -0.5$ meV, $m_C = 3\times10^{-5}m_e$, $\tau_p = 4$ ps, $\tau_x = 300$ ps, $\gamma, \eta = 0$, $g = 2\times10^{-2}$ meV μm^2, $\tilde{g} = g$, $\hbar R = 2.6\times10^{-3}$ meV μm^2, $W = 12.5\mu$m, $T_{pulse} = 50$ fs, $\Delta\omega = 0$, $n_R = 0$, $W = 12.5\mu$m, $T_{pulse} = 50$ fs (fs-pulse case) or $T_{pulse} = 2$ ps (ps-pulse case).

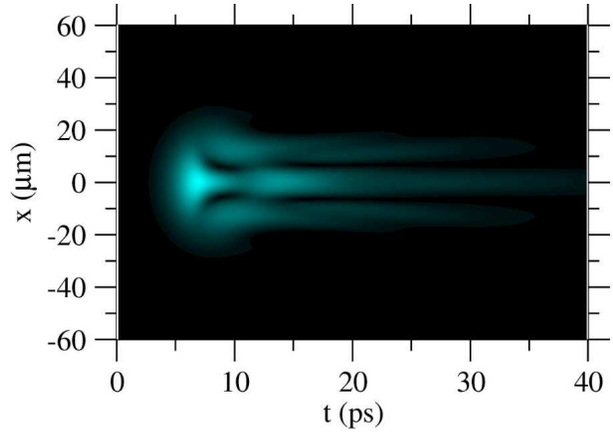

Figure S9: Evolution of the photon field intensity in the model with k-dependent nonlocal reduction of the Rabi coupling. Parameters are the same as in Fig. S8 (for ps pulse excitation at the LP branch) with $a = 4$ and $k_c = 0.2\mu\text{m}^{-1}$.

k_c^{-1}. Figure S9 shows an example of self-focusing in this model in the case of picosecond LP branch excitation. In the case of femtosecond excitation, the results are similar to the ones obtained with the previous model.

While this model provides a good agreement with experiments performed at different settings, its justification is not straightforward. While the k-dependent reduction of Rabi coupling can be predicted by the simple model of phase space filling or exchange effects[S8], it occurs at k vectors comparable to the inverse exciton Bohr radius a_B^{-1}. The dependence of the Ω_R on momentum for k comparable to μm^{-1} requires an existence of correlations over distances much larger than the exciton radius, for which we see no rationale in the mean-field framework. An explanation along

these lines is thus thwarted in a straightforward model and would require a drastic reconsideration of the physics of polaritons based on the mean-field approximation and perturbation theory in the exciton basis. In the close vicinity of the Mott transition, the description in terms of the dilute exciton gas may become questionable, and collective effects of strongly-correlated quantum gases could be required instead. Indeed, BCS-related physics is expected to occur close to the phase space filling threshold[S12]. Such an interpretation cannot be excluded and would open a new page of the field, but it is, however, much beyond the scope of this text.

II. LOCALISATION BY THE RESERVOIR

The exciton reservoir is another possible candidate to explain the redistribution of the polariton condensate. A conceivable scenario involves the creation of a ring of reservoir excitons around the center of the pumping spot, which subsequently creates a backflow of polariton waves, interfering constructively in the center and giving rise to the strong intensity peak. Such a model consists of the photon, exciton, and reservoir fields, similar to Ref.[S13], but treating coherent photons and excitons with separate fields:

$$\begin{aligned} i\hbar\frac{\partial\phi}{\partial t} &= -(1-iA)\frac{\hbar^2}{2m_C}\nabla^2\phi + \frac{\hbar\Omega_R}{2}\chi - \frac{i\hbar}{2\tau_p}\phi + F(\mathbf{r},t)\,, \\ i\hbar\frac{\partial\chi}{\partial t} &= \frac{\hbar\Omega_R}{2}\phi - i\delta\chi + g|\chi|^2\chi + \tilde{g}n_\mathrm{R}\chi + i\frac{\hbar}{2}\left(Rn_\mathrm{R} - \frac{1}{\tau_x}\right)\chi\,, \\ \frac{\partial n_\mathrm{R}}{\partial t} &= -\left(\frac{1}{\tau_x} + R|\chi|^2\right)n_\mathrm{R}\,, \end{aligned} \tag{S3}$$

where A is the energy relaxation constant, $F(\mathbf{r},t) = F_0 \mathrm{e}^{-\mathbf{r}^2/2W^2 - t^2/2T_{pulse}^2 - i\Delta\omega t}$ is the pumping field and with an initial reservoir density $n_R(\mathbf{r}, t=0) = n_0 \mathrm{e}^{-\mathbf{r}^2/2W^2}$. In this simple model, the backscattering from the condensate to the reservoir is not taken into account, but the initial reservoir density is assumed to be excited by the incoming pulse.

A numerical simulation of this model is shown in Fig. S10. The depletion in the center of the reservoir is created due to the stimulated scattering to the condensate, which is faster in the center, where the condensate density is larger. The bright density peak is then created because the polariton waves emitted form the remaining ring-shaped reservoir "focus" in the center. While the main feature of the experiment is thus reproduced, there are several problems with quantitative features: (a) the central peak appears much later than is observed in the experiment and (b) the bending of the Rabi oscillations is initially in the incorrect direction (backwards in the center). There are even more serious conceptual difficulties: (c) in such a model, the peak cannot move "ballistically", as is observed in the experiment if the excitation pulse is injected at an angle, since the reservoir would stay essentially in the position where it is created. (d) The peak persists when resonantly exciting the lower branch, which is expected to produce little or no reservoir excitons. (e) Finally, the effect does not show any strong polarization dependence. In the regime of quasiresonant

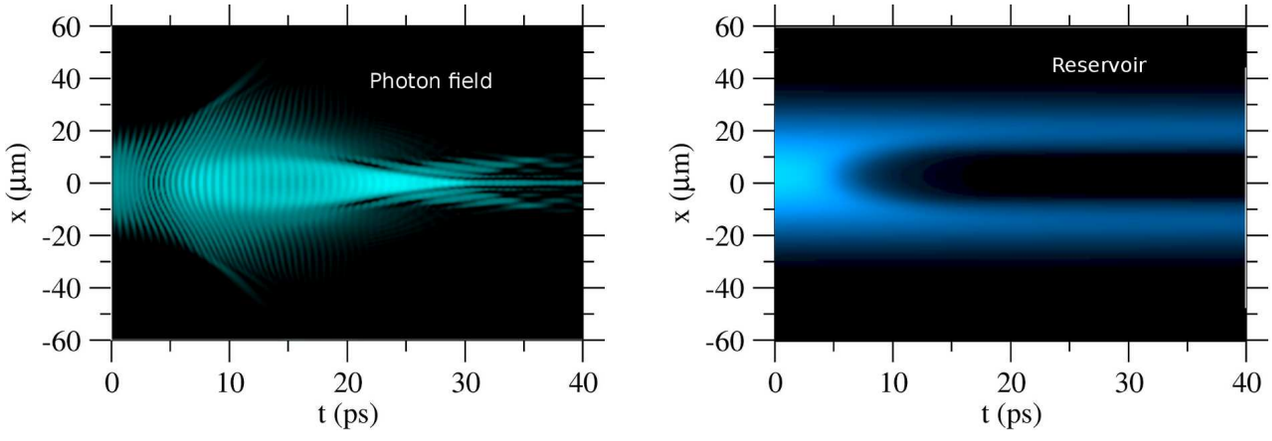

Figure S10: Evolution of the photon field intensity and reservoir density in the reservoir-ring model. Parameters are $A = 0$, $\delta = 0$, $m_C = 5 \times 10^{-5} m_e$, $\hbar\Omega_R = 6$ meV, $\tau_p = 2.5$ ps, $\tau_x = 300$ ps, $g = 12 \times 10^{-3}$ meV μm^2, $\tilde{g} = 2g$, $\hbar R = 2.6 \times 10^{-3}$ meV μm^2, $W = 12.5\mu$m, $T_{pulse} = 50$ fs, $\Delta\omega = 0$.

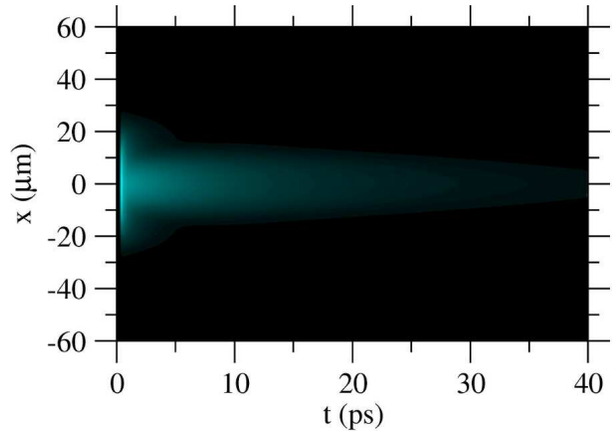

Figure S11: Evolution of the photon field intensity in the model with dark excitons. Parameters are the same as in Fig. S10, except $m_{LP} = 3 \times 10^{-5} m_e$, $\tau_p = 4$ ps, $\gamma_x = 0.4$ μm^2 ps^{-1}, $\gamma_d = 0.02$ μm^4 ps^{-1}, $g = 2 \times 10^{-2}$ meV μm^2, $n_0 = 0$.

pulsed excitation we expect the reservoir to be polarised as the typical exciton spin-relaxation time in our system is supposed to be long compared to the characteristic time scale of the Rabi-oscillations and collapse dynamics

Variations on this theme are possible. For instance, one can assume the intermission of dark excitons. Since the coupling is incoherent and assuming the exciton mass as infinite, which allows to treat dark excitons as a density field, their effect can be modeled by the following equations:

$$i\hbar\frac{\partial\psi}{\partial t} = \left(-\frac{\hbar^2}{2m_{LP}}\nabla^2 - \frac{i\hbar}{2\tau_p} - i\gamma|\psi|^2 + i\gamma_d n_{\rm dark}^2 + g\left(|\psi|^2 + n_{\rm dark}\right)\right)\psi + F(\mathbf{r},t), \tag{S4}$$

$$\frac{\partial n_{\rm dark}}{\partial t} = \gamma|\psi|^4 - \gamma_d n_{\rm dark}^2|\psi|^2.$$

A numerical simulation of this model is shown in Fig. S11. The scattering to polaritons creates a hole in the Gaussian distribution of excitons. The flow towards the hole can create a localization, however, the effect is not as clear as in the experiment: the localization is rather broad and has a low intensity.

III. ATTRACTIVE INTERACTIONS BETWEEN EXCITONS

The interaction constant in the Gross-Pitaevskii equations, and variants, that describe the polariton dynamics is positive, as indeed same-spin excitons are largely believed to be repulsive, but several effects could potentially give rise to attractive interactions, as we discuss shortly. Since we actually observe a real-space collapse, it is instructive to simply assume attractive interactions between polaritons. In this case self-focusing is indeed possible for a positive effective mass. The model is identical to the one above, Eqs. (S1), but with $g < 0$. We do not include the reservoir excitons that we have seen can be ruled out on several grounds. A result of numerical simulation is shown in Fig. S12. As expected, the high intensity peak appears due to self-focusing.

While some features of the experiment are well reproduced in this model, the existence of attractive polariton interactions is highly questionable. Potentially the strongest effect in this sense is the indirect exchange through the biexciton state, but this occurs only for opposite spins, while we did not observe any strong spin dependence of the focusing effect in the experiment. The other possible sources of attractive interaction, such as the indirect exchange[S14–S16], or Van der Waals interactions appear to be negligible for the low-momentum excitons created by resonant pumping[S16]. It was also recently observed that the sign of the interactions may change to negative at large polariton momenta[S15], and other effects could similarly give rise to polariton attraction[S15,S16], but the proposed configurations are difficult to fit in with our experiment. The change of sign of the polariton interactions with no further justification is thus not tenable and would be in conflict with a large literature that successfully describes various experimental regimes on a physically well motivated assumption of repulsive interactions.

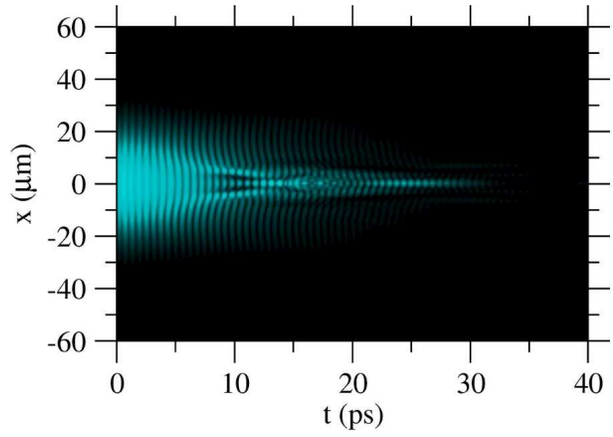

Figure S12: Evolution of the photon field intensity in the model with attractive polariton-polariton interactions. Parameters are the same as in Fig. S10, except $A = 0.1$, $\delta = 3$ meV, $g = -12 \times 10^{-3}$ meV μm^2, $\tilde{g} = 2|g|$, $\hbar R = 4.6 \times 10{-}3$ meV μm^2.

IV. COLLECTIVE POLARON EFFECT

We now conclude this series of possible models to reproduce the real-space collapse of the polariton condensate with the one model that we found could stand as an explanation for the observed effect.

When the exciton density is large enough, as in the case of pulsed excitation, the macroscopic occupation of the ground state with excitons may lead to enhancement of the exciton-phonon interaction that produces a cooling of the excitonic reservoir against its blueshift due to their attraction[S17,S18]. The corresponding released energy is transfered to the crystal lattice via acoustic phonons. Another plausible mechanism of heating is through the polariton-polariton Auger process followed by emission of the cascade of acoustic phonons as discussed by Klembt *et al.*[S19]. In any case, a local heating may occur which leads to a band-gap narrowing, a variation of the exciton-photon detuning and a redshift of the lower polariton branch. The latter effect may lead to self-focusing of the polariton condensate. Such an effect can be referred to as a "collective polaron effect". Formally, it can be described by the modulation of the exciton energy through a retarded function:

$$E_X(t) = -\frac{\beta}{\tau_X} \int_{-\infty}^{t} |\chi(\mathbf{r}, t')|^4 \, e^{-\frac{t-t'}{\tau_X}} \, dt', \tag{S5}$$

where β characterises the magnitude of band-gap renormalization and τ_X is the characteristic heat relaxation time in the crystal lattice. Both β and τ_X are fitting parameters. The fourth power of the exciton wavefunction $\chi(\mathbf{r}, t')$ under the integral accounts for the quadratic dependence of the polariton Auger process on the concentration of polaritons. The dynamics of the system is governed by the initial pumping strength. The Rabi oscillations generally have an anharmonic behavior due to the changes of the bare exciton energy and the interplay between the blueshift $g|\chi|^2$ and the redshift $E_X(t)$. The effective frequency of these oscillations is then determined by $\Omega_{\text{eff}} = \sqrt{\Omega_R^2 + (\Delta - g|\chi|^2)^2}$[S20]. In addition to the change in detuning, at larger population densities close to the Mott transition, the coupling Ω_R itself would be reduced, resulting from the change of the exciton oscillator strength due to the exciton phase space filling[S8]. The result of the numerical simulation of Eqs. (S1) with an Eq. (S5) dependence is shown in Fig. S13. At the initial stage, the Rabi oscillations between photon and exciton states are seen. The dependence of the oscillations frequency on the local detuning results in appearance of the radial waves spreading from the center of the spot. The modified density-dependent value of the Rabi frequency allows to reproduce some retardation of their motion in the spot center. When the density decreases due to the photonic decay, the direction of the wave-spreading changes. In addition, the heating reservoir forms a potential well, in which the polaritons are trapped through their excitonic fraction, that results in a stabilization of both excitonic and photonic components of the polariton flow. Further dynamics exibits the decay of both components of the polariton many-body wavefunction. One can see the typical behavior of the sharply localised peak appearance extracted at different pumping power, which is modeled by setting increasing amplitude of F_p in Eq. (S1). The results are shown in Fig. S14. The photonic phase component is plotted in Fig. S15.

In the present model as well, we assume that the incoherent reservoir is either completely empty or does not play any role. This assumption is certainly valid in the case of selective picosecond excitation of the lower polariton (LP) branch. We note also that the weak-coupling saturable optical nonlinearity could arise from instantaneous effects or

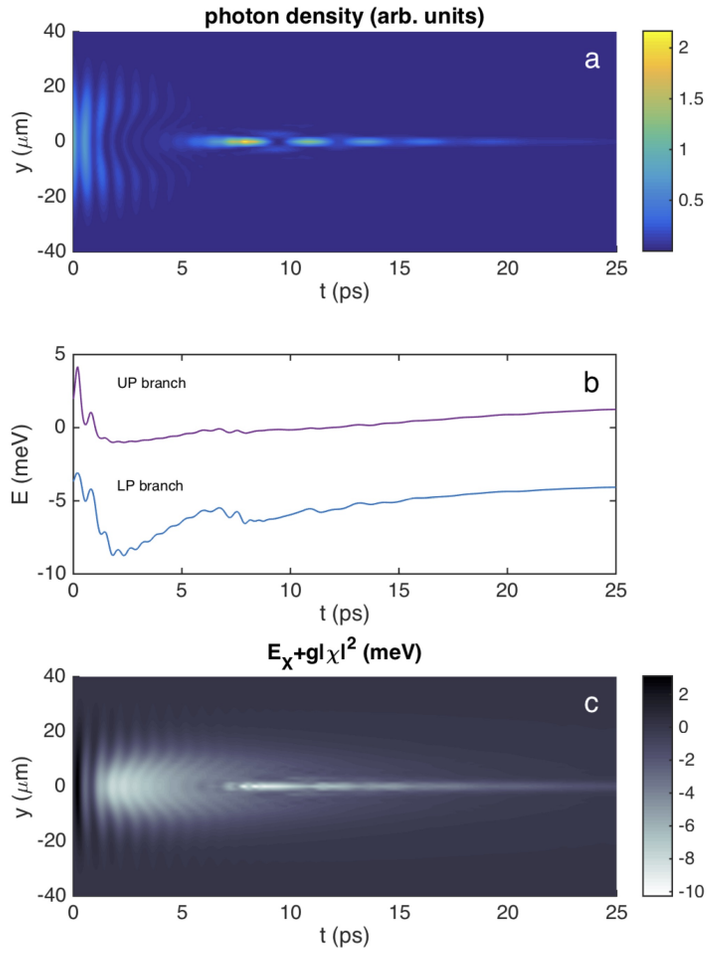

Figure S13: (a) Time-space chart of the photonic fraction intensity distribution. (b) The time dependence of the local energies of the upper polariton and lower polariton branches. The time-space chart of the effective exciton potential is shown in panel (c). Parameters used in calculations are $\Omega_R = 2\pi/(0.8\text{ ps})$, $\Delta = -1$ meV, $m_C = 3\times10^{-5}$, $\tau_C = 4$ ps, $\tau_X = 8$ ps, $g = 2\cdot10^{-2}$ meV μm^2, $\beta = g/n_{\text{sat}}$, $n_{\text{sat}} = 3\times10^{10}$ cm^{-1}. The pumping field is described by a fs-pulse with $W = 12.5$ μm, $T_{\text{pulse}} = 50$ fs, $E_p = 0$, and a variable amplitude F_p (see text).

sample heating[S21]. The instantaneous part, however, provides only defocusing nonlinearity for excitation below the band edge, as follows from the nonlinear Kramers-Kronig relations[S21,S22]. Heating generally leads to redshift which corresponds to focusing nonlinearity but has a longer response time.

In conclusions, while there is no compelling argument that impose the collactive polaron effect as the mechanism causing the collapse of the polariton condensate, our simulations show that it is a reasonable candidate, when other more straightforward scenarios fail to provide even a qualitative agreement or demand assumptions too strong to be justified. It is not excluded that more exotic many-body physics is at play, such as a variation of the BCS mechanism, holding the Bosonic condensate together in a way similar as the superconducting phase molds the Fermion liquid, or a dynamical Casimir effect[S23] pulling non-zero-momentum particles out of the suddenly hit polariton vacuum. We feel that it is left to theorists and further investigations to elucidate which exact physics is causing the peculiar phenomenology that we report.

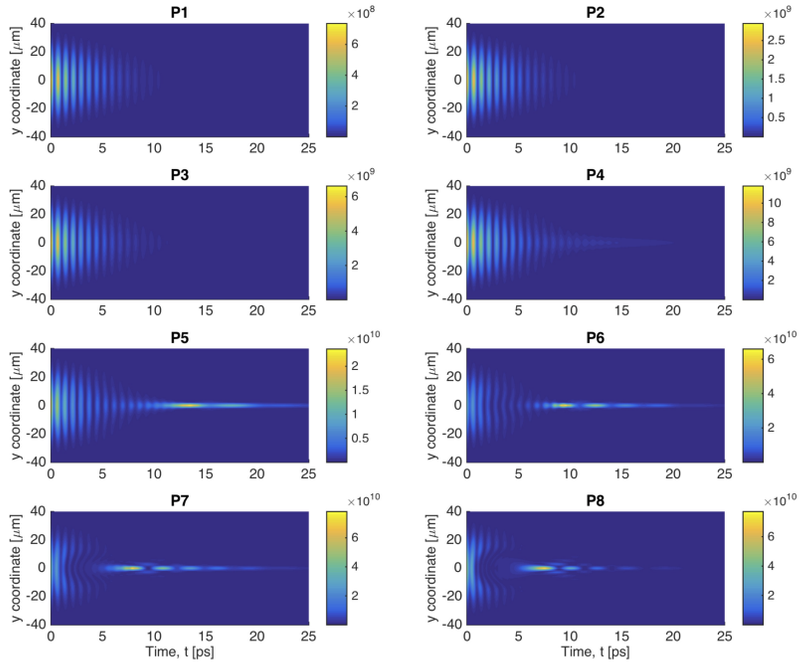

Figure S14: Calculated time-space charts of the photonic component of the polariton wavefunction as in Fig. S13(a). The number of polaritons increases proportionally from P_1 to P_8. Other parameters are the same as in the caption of Fig. S13.

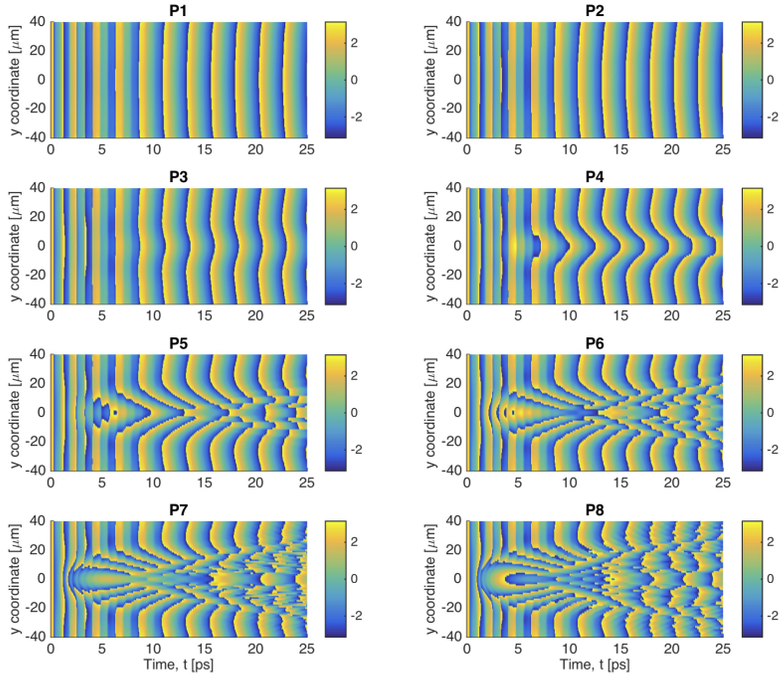

Figure S15: Calculated time-space chart of the photonic phase at different powers if using a pulsed excitation, as in Fig. S14.

Description of videos S1-S3

Movies S1-S2. The movies show the complete imaging of the fluid dynamics over a timespan of 40 ps with a timestep of 50 fs, as 3D and 2D maps, respectively. This gives a direct view of the ultrafast superfluid dynamics, combining Rabi oscillations and the central collapse along with the other phenomena described in the text and in Fig. 1-3.
Movie S3. Same as the previous movies but now showing the corresponding radial cross section of the polariton density $|\Psi(y)|^2$. As an interesting detail, it is possible to observe how the initial expansion in the first few ps is happening during the half-periods of the Rabi cycles where there is a low photonic density (i.e., a high excitonic one).
Link to supplementary movies

[S1] Ciuti, C., Schwendimann, P. & Quattropani, A. Theory of polariton parametric interactions in semiconductor microcavities. *Semiconductor Science and Technology* **18**, S279–S293 (2003). http://stacks.iop.org/0268-1242/18/i=10/a=301.

[S2] Carusotto, I. & Ciuti, C. Probing microcavity polariton superfluidity through resonant rayleigh scattering. *Phys. Rev. Lett.* **93**, 166401 (2004). http://link.aps.org/doi/10.1103/PhysRevLett.93.166401.

[S3] Steger, M. *et al.* Long-range ballistic motion and coherent flow of long-lifetime polaritons. *Phys. Rev. B* **88**, 235314 (2013). http://link.aps.org/doi/10.1103/PhysRevB.88.235314.

[S4] Amo, A. *et al.* Collective fluid dynamics of a polariton condensate in a semiconductor microcavity. *Nature* **457**, 291–5 (2009). http://dx.doi.org/10.1038/nature07640.

[S5] Amo, A. *et al.* Superfluidity of polaritons in semiconductor microcavities. *Nature Physics* **5**, 805–810 (2009). http://dx.doi.org/10.1038/nphys1364.

[S6] Sich, M. *et al.* Observation of bright polariton solitons in a semiconductor microcavity. *Nature Photonics* **6**, 50–55 (2012). http://dx.doi.org/10.1038/nphoton.2011.267.

[S7] Carusotto, I. & Ciuti, C. Quantum fluids of light. *Rev. Mod. Phys.* **85**, 299–366 (2013). http://link.aps.org/doi/10.1103/RevModPhys.85.299.

[S8] Schmitt-Rink, S., Chemla, D. S. & Miller, D. A. B. Theory of transient excitonic optical nonlinearities in semiconductor quantum-well structures. *Phys. Rev. B* **32**, 6601–6609 (1985). http://link.aps.org/doi/10.1103/PhysRevB.32.6601.

[S9] Rochat, G. *et al.* Excitonic bloch equations for a two-dimensional system of interacting excitons. *Phys. Rev. B* **61**, 13856–13862 (2000). http://link.aps.org/doi/10.1103/PhysRevB.61.13856.

[S10] Kwong, N. H., Takayama, R., Rumyantsev, I., Kuwata-Gonokami, M. & Binder, R. Third-order exciton-correlation and nonlinear cavity-polariton effects in semiconductor microcavities. *Phys. Rev. B* **64**, 045316 (2001). http://link.aps.org/doi/10.1103/PhysRevB.64.045316.

[S11] Luk, M. H. *et al.* Transverse optical instability patterns in semiconductor microcavities: Polariton scattering and low-intensity all-optical switching. *Phys. Rev. B* **87**, 205307 (2013). http://link.aps.org/doi/10.1103/PhysRevB.87.205307.

[S12] Keeling, J., Eastham, P. R., Szymanska, M. H. & Littlewood, P. B. BCS-BEC crossover in a system of microcavity polaritons. *Phys. Rev. B* **72**, 115320 (2005). http://link.aps.org/doi/10.1103/PhysRevB.72.115320.

[S13] Wouters, M. & Carusotto, I. Excitations in a nonequilibrium bose-einstein condensate of exciton polaritons. *Phys. Rev. Lett.* **99**, 140402 (2007). http://link.aps.org/doi/10.1103/PhysRevLett.99.140402.

[S14] Ciuti, C., Savona, V., Piermarocchi, C., Quattropani, A. & Schwendimann, P. Role of the exchange of carriers in elastic exciton-exciton scattering in quantum wells. *Phys. Rev. B* **58**, 7926–7933 (1998). http://link.aps.org/doi/10.1103/PhysRevB.58.7926.

[S15] Vishnevsky, D. V. & Laussy, F. Effective attractive polariton-polariton interaction mediated by an exciton reservoir. *Phys. Rev. B* **90**, 035413 (2014). http://link.aps.org/doi/10.1103/PhysRevB.90.035413.

[S16] Vladimirova, M. *et al.* Polariton-polariton interaction constants in microcavities. *Phys. Rev. B* **82**, 075301 (2010). http://link.aps.org/doi/10.1103/PhysRevB.82.075301.

[S17] Ivanov, A. L., Littlewood, P. B. & Haug, H. Bose-einstein statistics in thermalization and photoluminescence of quantum-well excitons. *Phys. Rev. B* **59**, 5032–5048 (1999). http://link.aps.org/doi/10.1103/PhysRevB.59.5032.

[S18] Porras, D., Ciuti, C., Baumberg, J. J. & Tejedor, C. Polariton dynamics and bose-einstein condensation in semiconductor microcavities. *Phys. Rev. B* **66**, 085304 (2002). http://link.aps.org/doi/10.1103/PhysRevB.66.085304.

[S19] Klembt, S. *et al.* Exciton-polariton gas as a nonequilibrium coolant. *Phys. Rev. Lett.* **114**, 186403 (2015). http://link.aps.org/doi/10.1103/PhysRevLett.114.186403.

[S20] Voronova, N., Elistratov, A. & Lozovik, Y. Detuning-controlled internal oscillations in an exciton-polariton condensate. *arXiv preprint* 1503.04231 (2015). http://arxiv.org/abs/1503.04231.

[S21] Taranenko, V., Slekys, G. & Weiss, C. Spatial resonator solitons. In Akhmediev, N. & Ankiewicz, A. (eds.) *Dissipative Solitons*, vol. 661 of *Lecture Notes in Physics*, 131–160 (Springer Berlin Heidelberg, 2005). http://dx.doi.org/10.1007/10928028_6.

[S22] Kost, A. Resonant optical nonlinearities in semiconductors. In Garmire, E. & Kost, A. (eds.) *Nonlinear Optics in Semiconductors I*, vol. 58 of *Semiconductors and Semimetals*, 1–53 (Academic Press, 1998). http://www.sciencedirect.com/science/article/pii/S0080878408627209.

[S23] Koghee, S. & Wouters, M. Dynamical casimir emission from polariton condensates. *Phys. Rev. Lett.* **112**, 036406 (2014). http://link.aps.org/doi/10.1103/PhysRevLett.112.036406.